# Point Focus Acoustic Materials Signature V(z) of Anisotropic Solids

M. Deschamps and A.G. Every#
Laboratoire de Mécanique Physique, URA C.N.R.S. no. 867
Université de Bordeaux I, 351 Cours de la Libération,
33405 Talence-Cedex,
France

Tel (33) (0) 5 56 84 62 26
Fax (33) (0) 5 56 84 69 64
E-mail deschamps@lmp.u-bordeaux.fr

#On leave from University of the Witwatersrand, Johannesburg, South Africa

**ABSTRACT**

The purpose of this paper is to show that point focus $V(z)$ signals obtained on anisotropic solids are dominated by a small number of principal surface wave rays, which correspond to directions in which the surface wave slowness is stationary. In consequence, the inverse problem becomes more manageable. As an example, the computed $V(z)$ curve for the (001) surface of Cu is analyzed, and is found to be the superposition of 4 dominant periods. Two of these are associated with the RW, one corresponding to the [100] direction where the RW slowness is a maximum, and the other to an oblique direction where the RW slowness is a minimum. The other two periods correspond to a maximum and a minimum in the PSAW slowness.

## Introduction

In point focus-beam (PFB) acoustic microscopy (AM) of anisotropic solids the acoustic materials signature $V(z)$ is given by [1,2,3]:

$$V(z) = \int_0^{\theta_m} P(\theta)\, \overline{R}(\theta)\, \exp(-2ikz\cos\theta)\, d\theta \ , \tag{1}$$

where $P(\theta)$ is the aperture function of the lens, assumed here to be axially symmetric and dependent only on the polar angle, $\theta$, measured from the surface normal,

$$\overline{R}(\theta) = \frac{1}{2\pi}\int_0^{2\pi} R(\theta,\varphi)\, d\varphi \ , \tag{2}$$

is the complex mean reflectance function of the surface (i.e. the reflectivity $R(\theta,\varphi)$ averaged over the azimuthal angle $\varphi$), $k=2\pi f/v$ is the wave number in the fluid coupling medium, $f$ is the frequency, $v$ is the sound speed in the fluid, and $z$ is the distance of the focal point of the lens from the specimen surface. A common perception is that the folding of the entire $\varphi$ dependence of the reflectivity into the mean reflectance function $\overline{R}(\theta)$, and thereby a single $V(z)$ signal washes out much of the detailed information on the surface dynamics, and renders

the inverse problem of recovering elastic constants or other physical parameters precarious. Partly for that reason, most AM investigations of anisotropic solids are conducted with line focus beam (LFB) AM [4,5] or non-axially symmetric PFB lenses. [6,7,8] In LFB AM individual $V_{(z)}$ curves are obtained for each value of $\varphi$, yielding the angular dependence of the Rayleigh (RW) and, depending on the circumstances, pseudo surface acoustic wave (PSAW) and/or the lateral wave velocities. The purpose of this paper is to draw attention to the fact that PFB $V_{(z)}$ signals obtained on anisotropic solids are dominated by a small number of principal surface acoustic wave (SAW) rays, which are associated with directions in which the RW or PSAW phase slowness is stationary. Aided by this fact, the extraction of materials information from a PFB $V_{(z)}$ curves becomes a more manageable problem. We illustrate this fact using as an example the computed surface dynamics, reflectivity and associated $V_{(z)}$ curve for the (001) surface of copper. It turns out that the spatial Fourier spectrum of $V_{(z)}$ contain four dominant periods. Two of these are associated with the RW, one corresponding to the [100] direction where the RW slowness is a maximum, and the other to an oblique direction where the RW slowness is a minimum. The other two periods correspond to a maximum and a minimum in the PSAW slowness. In spite of the damping and consequent broadening of the surface wave velocities by the fluid (water) loading of the Cu surface, the principal velocities can still be obtained to better than 0.25% accuracy from the computed $V_{(z)}$ curve.

**Reflectivity of Anisotropic Solid**

Figure 1 shows the angular dependence of the magnitude $|R|$ and phase $\Phi$ of the reflectivity $R_{(\theta)}$ for the water loaded Cu(001) surface for (010) orientation of the sagittal plane (no azimuthal averaging here). Each feature, at angle $\theta$, is in one-to-one correspondence with a surface wave slowness

$$s = sin(\theta) / v_{water} \ , \tag{3}$$

where $v_{water}$ is the sound speed in water, taken as 1.509 mm/µs in this paper. The features labeled a, b, c and D correspond respectively to the longitudinal lateral wave slowness $s = \sqrt{\rho / C_{11}}$, the transverse lateral wave slowness $s = \sqrt{\rho / C_{44}}$, the threshold bulk wave slowness (for which $s$ is inclined to the surface but with the corresponding ray velocity $V$ parallel to the surface), and the RW slowness. Beyond c there is no bulk wave into which the incident wave can be transmitted, and so $|R_{(\theta)}| = 1$. The Rayleigh wave slowness is marked by a rapid decrease in the phase $\Phi_{(\theta)}$ by almost $2\pi$, and there are sharp kinks in $\Phi_{(\theta)}$ at a, b and c.
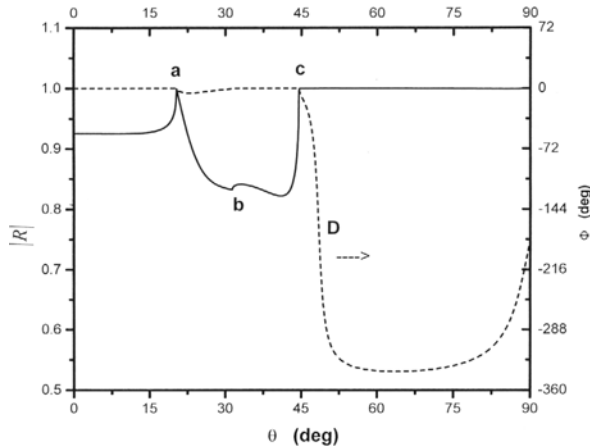


Figure 1. $R_{(\theta,\varphi=0°)}$ for the Cu(001) surface.     Figure 2. $R_{(\theta,\varphi=45°)}$ the Cu(001) surface.
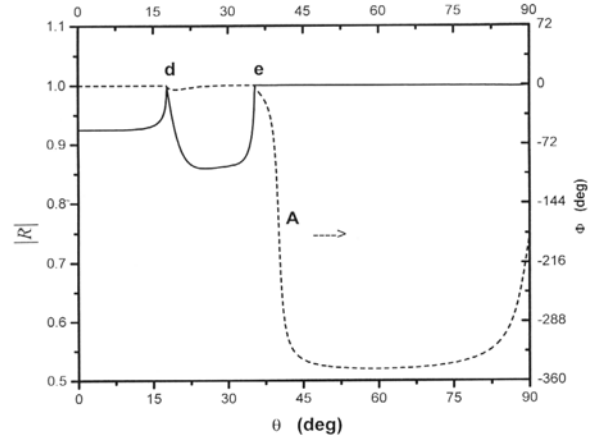
Figure 2 shows the angular dependence of $R_{(\theta)}$ for the water loaded Cu(001) surface for ($\bar{1}$10) orientation of the sagittal plane. The features labeled d, e and A correspond respectively to the longitudinal lateral wave slowness $s = \sqrt{2\rho / (C_{11} + C_{12} + 2C_{44})}$, the threshold slowness for sagittally polarized displacements, and the PSAW slowness. The PSAW in this symmetry plane is a pure two component supersonic SAW. The

bulk wave continuum of SH polarized waves extends some way beyond the PSAW slowness, but is uncoupled from the incident pressure wave in the fluid. The two reflectivity curves in Figs. 1 and 2 differ appreciably, and there is considerable variation in the reflectivity curves for the sagittal planes between (010) and ($\bar{1}$10).
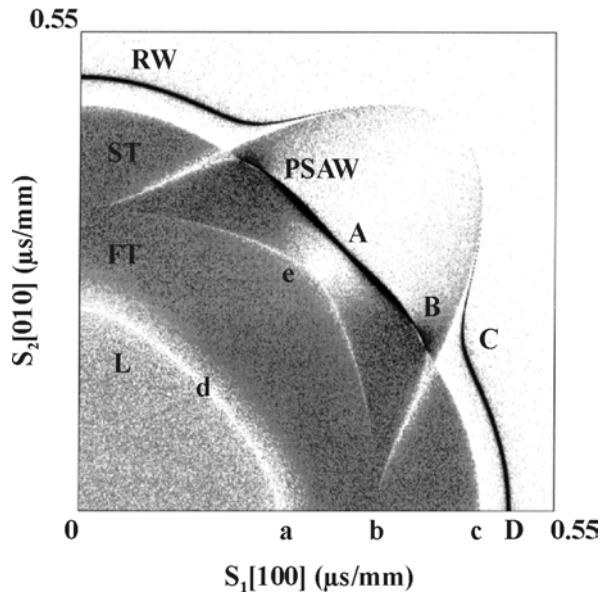


Figure 3.  *Im $G_{33}(s_{//})$ for the Cu(001) surface.*
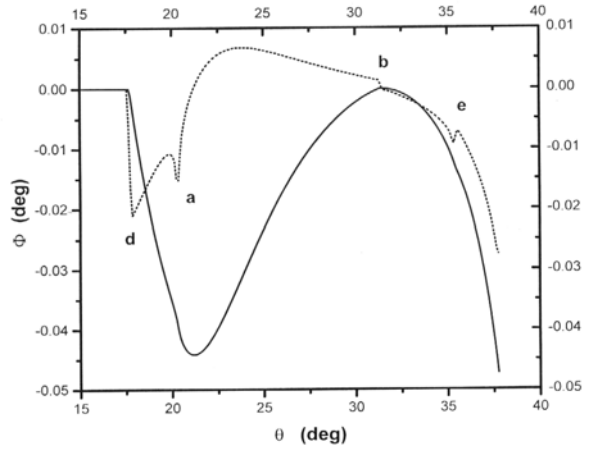


Figure 4.  $\Phi$ ——— and $\dfrac{d\Phi}{d\theta}$ - - - of Cu(001) loaded by low acoustic impedance fluid.
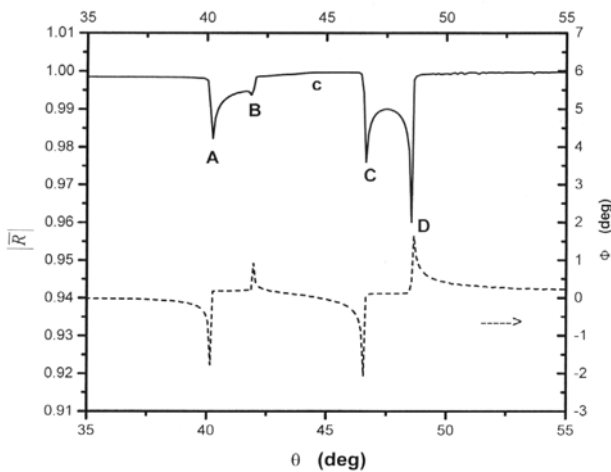


Figure 5.  $\left| R \right|$ ——— and $\Phi$ - - - - in a different angular range.
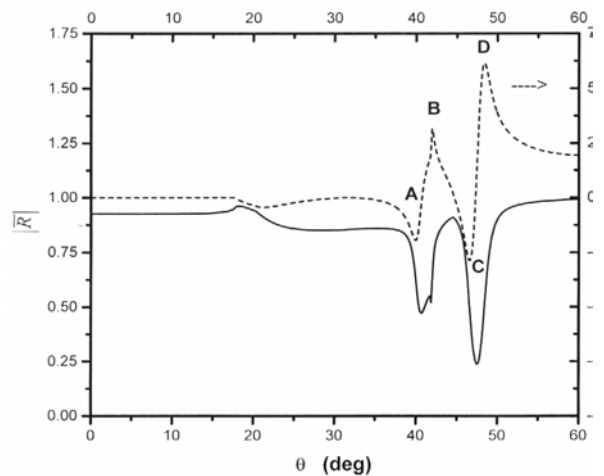


Figure 6.  *$\overline{R}(\theta)$ for the water-loaded Cu(001) surface.*

A global view of the surface dynamics of the Cu(001) surface is provided by Fig. 3, which shows, in gray scale,  *Im $G_{33}(s_{//})$*, the imaginary part of the Fourier domain surface dynamic response function for force and displacement normal to the surface. The darkness of the image is a measure of the weighted density of bulk and surface modes. The lateral waves show up as lighter lines against a dark background, the threshold slownesses form the boundary between dark and bright (subsonic) regions, and the RW and PSAW are the intense narrow dark lines. A small amount of damping has been incorporated in the calculations to give the RW a finite width

and render it visible in the diagram. The seven symmetry plane slownesses a, b, c, d, e, D and A are evidently all limiting values of SAW slownesses with variation of the angle $\varphi$ in the surface, as one would expect on symmetry grounds. In addition there are two non-symmetry limiting slowness directions, C in a direction 21° from the <100> axis, where the RW slowness is a minimum, and B in a direction 28° from the <100> axis, where the PSAW slowness is a maximum. Table 1 lists all the limiting slownesses $s_{//}$ for the Cu(001) surface, and related information which is discussed below.

| | Slowness | $\varphi$ (deg) | $\theta$ (deg) | $s_{//}$ (µs/mm) | $v_{//}$ (mm/µs) | $\Delta z$ (mm) | $v_{SAW}$ (mm/µs) |
|---|---|---|---|---|---|---|---|
| a | L max | 0 | 20.3 | 0.230 | 4.35 | | |
| b | FT min | 0 | 31.3 | 0.344 | 2.90 | | |
| c | ST max | 0 | 44.4 | 0.464 | 2.16 | | |
| d | L min | 45 | 17.7 | | 4.96 | | |
| e | FT max | 45 | 35.4 | 0.384 | 2.61 | | |
| A | PSAW min | 45 | 40.15 | 0.4273 | 2.340 | .01427 | 2.343 |
| B | PSAW max | 28 | 41.95 | 0.4430 | 2.257 | .01299 | 2.250 |
| C | RW min | 21 | 46.55 | 0.4811 | 2.079 | .01082 | 2.085 |
| D | RW max | 0 | 48.60 | 0.4971 | 2.012 | .00993 | 2.014 |

Table 1: Stationary slownesses and principal rays rays for the Cu(001) surface. $s_{//}$ is obtained from Eq. (3) and $v_{//} = 1/s_{//}$. $\Delta z$ is from the FFT of $V(z)$ and $v_{SAW}$ is from Eq. (4).

Figure 3 has been calculated for the free Cu(001) surface. With fluid loading the RW and PSAW become appreciably damped through being able to radiate their energy into phase matched bulk waves in the fluid, and a similar calculation to Fig. 3 shows the sharp RW and PSAW curves broadened into bands. Correspondingly, there is a finite rather than infinitesimal angular range over which $\Phi(\theta)$ undergoes its decrease by approximately $2\pi$. The same is not true for the lateral and threshold waves, which are characteristic features of the solid surface. These are independent of the fluid loading, and so remain sharp. The broadening of the RW and PSAW resonances, as we will see, are accompanied by only small net shifts in their slownesses, and so these slownesses can still be measured accurately. In calculating the mean reflectance function $\bar{R}(\theta)$, it is nevertheless illuminating to consider the limiting case of weak loading of the solid surface by a fluid of low acoustic impedance $Z_f$ compared with that of the solid, $Z_s$. Such would be the case, for instance, with air-coupled transduction.

Figure 4 shows, for loading by a hypothetical fluid of velocity that of water but one hundredth of its density and acoustic impedance, the phase $\Phi$ of $\bar{R}(\theta)$ in the angular range of the lateral waves a, b and d, and the threshold wave e, and Fig. 5, for a different range, shows $\Phi$ and $|\bar{R}|$ in the region of the RW and PSAW. Both the phase and magnitude of $\bar{R}(\theta)$ show characteristic singularities at the four limiting RW and PSAW slownesses, in the form of a discontinuity, with finite slope to one side and a power law type variation on the other side of the discontinuity. There is reversal of this singularity for a maximum vis-à-vis a minimum type stationary point. The sharp dips C and D in $|\bar{R}(\theta)|$ in Fig. 5 arise in the integration over an angular range throughout which $|R(\theta,\varphi)| = 1$. There is, however, pronounced variation of $\Phi(\theta,\varphi)$ in this range, and as a result $|\bar{R}(\theta)| < 1$ through phase cancellation. As the integration path, with variation of $\theta$, approaches tangency with the RW curve at the stationary point C or D there is a greater range of the integration path, where $\Phi(\theta,\varphi)$ differs markedly from 0 or $2\pi$, and this accounts for the sharp dips in $|\bar{R}(\theta)|$ at the stationary slownesses. The same considerations apply to the PSAW stationary slowness points. At each of the limiting slownesses of the lateral and threshold waves, $\Phi(\theta)$, has kink, i.e. discontinuous change in slope, which shows up more clearly in the dashed curve representing the derivative $\dfrac{d\Phi}{d\theta}$ in Fig. 4. The threshold c lies in the angular range of Fig. 5, and also takes the form of a kink in $\Phi(\theta)$. Figure 6 now shows the azimuthally averaged reflectivity $\bar{R}(\theta)$ for the

water-loaded Cu(001) surface (this is essentially the same as Fig. 11.10 of Ref.[1]). Even though $\bar{R}(\theta)$ differs markedly from the weak loading case, there are still clearly identifiable sharp peaks or troughs in $\Phi(\theta)$ occurring within 0.25% of the limiting slownesses for the RW and PSAW, and a kink at the L lateral slowness d.

**Point Focus** $V(z)$

Figure 7 now shows the calculated point focus $V(z)$ for the water loaded Cu(001) surface for an operating frequency of 225 MHz. Evidently there are several periods in the complicated variation of $V$ with $z$, and this becomes obvious from the fast Fourier transform (FFT) $F(k)$ of $V(z)$, shown in Fig. 8. In the wave number interval between 60 mm$^{-1}$ and 110 mm$^{-1}$, there are four pronounced peaks in $F(k)$, which correspond to spatial periods, $\Delta z = 1/k$, listed in Table 1. The corresponding SAW velocities, calculated by the standard ray model relation [1,2,3]

$$v_{SAW} = v_{water} / \sqrt{1 - \left(1 - \frac{v_{water}}{2f\Delta z}\right)^2},$$ 

(4)

are also shown in Table 1, and are seen to be in very good agreement with the limiting RW and PSAW velocities $v_{//}$ (to within 0.25% in all cases).
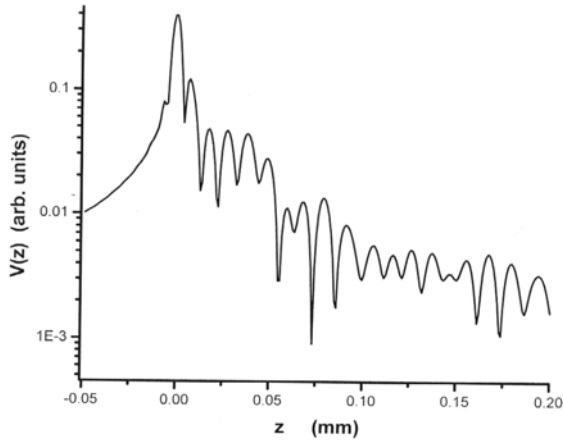


Figure 7. $V(z)$ for water loaded Cu(001) surface.
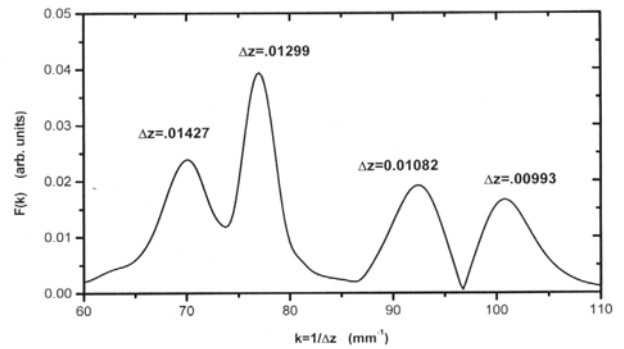


Figure 8. FFT $F(k)$ of $V(z)$.

**Ray Model Interpretation**

Figure 9 suggests a simple ray model interpretation of the principle ray idea discussed in this paper (a similar line of reasoning has been advanced by Kushibiki et al. [8]). The oscillations in $V(z)$, as is well known, can be considered to result from the interference of two (or more) rays. One is the ray along the axis of the lens, which is incident normally on the specimen surface, specularly reflected and retraces its path into the lens. The other is the ray which is incident on the surface at the Rayleigh angle

$$\theta_R = arcsin\left(v_{fluid}/v_{solid}\right),$$ 

(5)

exciting a phase matched leaky Rayleigh wave in the surface, which subsequently radiates back into the fluid. It is only the ray which is radiated from the diametrically opposite point to the point of incidence that ends up traveling directly up the lens and so is able to contribute to the signal. It is precisely this argument which for an isotropic solid or LFB AM of an anisotropic solid, leads to Eq. (4).
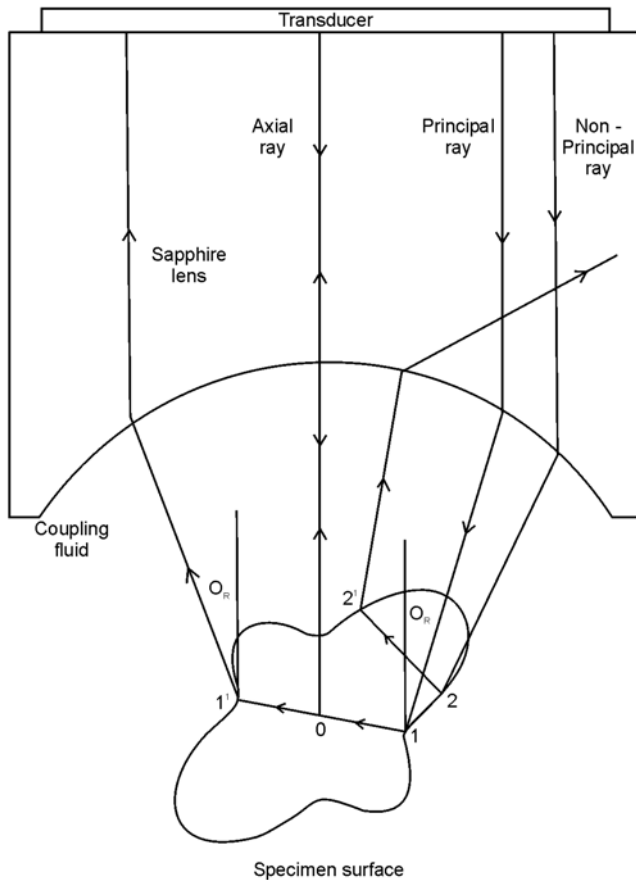
Figure 9. Ray model for the principal rays.

In the case of an anisotropic solid, there is a range of different Rayleigh incidence angles $\theta_R(\varphi)$, which depend on the azimuthal angle, and which correspond to rays incident on the surface along the non-circular curved path depicted schematically in Fig. 9. The surface wave which is excited at point 1, which is a point of stationary slowness not necessarily lying in a symmetry direction, has surface ray and slowness vectors which are parallel to each other (since the ray velocity is normal to the slowness curve), and so the ray passes through the origin 0 to arrive at the inversion point 1' where its radiation into the fluid ends up traveling directly up the lens, and contributes to $V_{(z)}$. The ray which is excited at the non stationary slowness point 2, on the other hand, veers off to the side (an effect known as beam walk off [7]) and does not pass through the origin to reach its symmetrically opposite point. Instead it arrives at the excitation contour at point 2', from where its radiation into the fluid does not end up passing directly up the lens. As a result, this ray does not contribute to $V_{(z)}$. Thus, only the stationary slowness points play a significant role in determining the form of $V_{(z)}$. The link between the ray model and the reflectivity approach is that the major contributions to the integral in Eq. (1) come from the neighborhood of angles $\theta$ where the phase of the integrand is stationary. Apart from the axial ray, these are the stationary slowness angles where $\Phi$ decreases most rapidly.

**Inverse Problems**

Possible approaches to the inverse problem of recovering elastic constants or other information on an anisotropic solid from the periods of a single $V_{(z)}$ curve will be discussed. The practical advantages of using point focus AM for anisotropic solids is that a single measured $V_{(z)}$ curve provides almost as much useful information as does an entire family of curves obtained by LFAM, and secondly, the technical difficulties of maintaining the focal line accurately parallel to the specimen surface are circumvented.

**References**

[1] Briggs A 1992, *Acoustic Microscopy* (Clarendon Press, Oxford)
[2] Zinin P V 2001, *Handbook of Elastic Properties of Solids, Liquids and Gases* Eds. Levy M, Bass H E and Stern R R Vol. I (Academic Press: New York) p.187
[3] Yu Z and Boseck S 1995, *Rev. Mod. Phys.* **67**, 863
[4] Kushibiki J, Ohkubo A and Chubachi N 1981, *Electron. Lett.* 17, 520
[5] Achenbach J D, Kim J O and Lee Y C 1995, in *Advances in Acoustic Microscopy* Vol. **I**, Ed. Briggs A (Plenum: New York) p.153
[6] Kushibiki J and Chubachi N 1985, *IEEE Trans. Son. Ultrason.* **SU32**, 189
[7] Hildebrandt J A and Lam L K 1983, *Appl. Phys. Lett.* **42**, 413
[8] Kushibiki J, Chubachi N and Tejima E 1989, *Proc. Ultrasonics International'89*, 736